MEASURING SNOW MECHANICAL PROPERTIES TYPICAL OF STORM SNOW INSTABILITIES

Benjamin Reuter[1,2,*], Neige Calonne[1,3], and Ed Adams[1]

[1] *Montana State University, Department of Civil Engineering, 205 Cobleigh Hall, Bozeman, MT 59717, U.S.A.*
[2] *WSL Institute for Snow and Avalanche Research SLF, Davos, Switzerland*
[3] *Météo-France – CNRS, CNRM-GAME, URA1357, CEN, Grenoble, France*

ABSTRACT: Dry snow slab avalanches release after failure has occurred in a weak layer below a cohesive snow slab. Typically, weak layers either consist of precipitation particles or persistent grain types. In view of forecasting, active times of such weak layers are significantly shorter for precipitation particles. Hence, studying the characteristics of storm snow instabilities in the field requires good timing and are challenging since the peak of these instabilities occurs most likely during or toward the end of a storm – when weather conditions hinder traditional field measurements.

To overcome these difficulties, we investigated storm snow instabilities based on cold-laboratory experiments. Demonstrated techniques allow layers of nature representative snow to be artificially created in the laboratory. We created different artificial snowpack made of a base layer, a weak layer, and a slab layer by either growing crystals or depositing sifted disaggregated particles. Weak layers of decomposing fragmented particles were created to mimic storm snow snowpack; persistent weak layers of surface hoar and facets were also created to allow comparisons. After some defined time lag we loaded snow samples in a mechanical testing apparatus in shear to measure displacement, strain and failure using an image correlation technique. Micro computed snow tomography and snow micropenetrometry captured the microstructural properties at and around the interface where failure occurred.

Our results show that the shear strain was concentrated in the weak layer. Failure occurred after plastic deformation. Measured values of shear strength and shear modulus were similar for the different the weak layers, and tended to increase after burial. This observation is most likely due to the growth of grain bonds occurring during isothermal metamorphism.

KEYWORDS: snow failure, snow mechanics, mechanical properties, snow instability, storm snow.

1. INTRODUCTION

During dry avalanche release, a failure in a weak layer initiates underneath a cohesive slab, forming a crack that propagates across a slope to finally detach a large snow slab (Schweizer et al., 2016). These processes of failure initiation and crack propagation take place in weak layers of precipitation particles or persistent grain types mainly.

Avalanche forecasts are rather short-term forecasts aiming at estimating the evolution of snow instability for the following hours, often based on observation data. Depending on the weak layer type, active times vary and are significantly shorter for precipitation particles than for persistent grain types. Hence, observing the characteristics of storm snow instabilities in the field requires good timing. Also, we often miss the peak of these instabilities because they most likely occur during or toward the end of a storm, when weather conditions likely hinder field observations.

Another approach, also amenable for forecasting, uses snow instability modelling and requires snow mechanical data resolving the structural and mechanical differences between slab and weak layers. Despite the anticipated influence of snow microstructure (e.g. Walters & Adams, 2012), current parameterizations of snow mechanical properties still mainly rely on density only.

To investigate how storm snow layers fail and what role microstructural differences between weak layers play, we tested small layered snow samples in the cold laboratory in shear. The samples had a weak layer of decomposing fragmented particles (DF) topped by a slab of sifted disaggregated grains. To compare with, we also made weak layers consisting of surface hoar (SF) and faceted crystals (FC). Using 2-D strain measurements we derived the fracture mechanical properties of the weak layers. Snow micropenetration was used to ascertain the snow microstructural properties of the weak stratigraphy.

* *Corresponding author address:*
Benjamin Reuter, Dept. of Civil Engineering, Montana State University, Bozeman MT, U.S.A.
email: reuter@slf.ch

2. METHODS

In a cold laboratory at -5°C, we prepared 26 layered samples containing a weak layer. We tested the layered samples in shear, recorded the fracture for analysis with digital image correlation (DIC) and measured the snow microstructure with the snow micro-penetrometer (SMP).

2.1 Procedure

Instead of natural snow we used artificially produced snow that resembles typical snow types found in nature. At the surface of a snow filled box representing a well-sintered base, we prepared a weak layer of 5 to 10 mm thickness. Then we sifted snow on top – simulating a slab which had four shear frames inserted. After letting the layers sinter for at least 30 min, up to 6 SMP measurements were taken around the first shear frame. Then, snow was removed from the around the shear frame perimeter to a depth below the frame of about 2 cm. One vertical sidewall was sprayed with a stochastic speckle pattern for digital image correlation (DIC) analysis. One measurement series consists of four such mechanical tests. These are associated with SMP measurements obtained from the region between the planar area outlined by the shear frames.

2.2 Weak layer preparation

The weak layer was either a surface hoar layer (SH) that was grown on the base layer or snow that was deposited by sifting disaggregated particles on that base. Surface hoar growth conditions were similar to Stanton et al. (2012). The particles we sifted on the base to form a weak layer were either decomposing fragmented dendritic particles (DF) artificially produced in a snow maker or rounding faceted crystals (FCxr). The faceted crystals were similar in morphology to surface hoar grown from vapor onto the cold chamber ceiling that we had swept prior to the experiment.

2.3 Snow micro-penetrometry

The snow micro-penetrometer (SMP) measures vertical signals of penetration resistance. Following the approach for signal interpretation suggested by Löwe and van Herwijnen (2012), snow microstructural parameters, namely element length, deflection at rupture and rupture force, are obtained. Based on these three microstructural properties, snow density can be derived with a parameterization as previously done by Proksch et al. (2014). Instead of using their coefficients, we derived a calibration specific to our SMP device based on density values obtained by micro-computed tomography.

2.4 Digital image correlation

A digital image correlation (DIC) technique provides a means to derive strain during deformation of the sample until failure. We obtained values of shear strain by averaging across the region concentrating the shear strain. We compared this area with near-infrared pictures (Figure 1) of the samples' sidewall clearly depicting the weak layer below the slab. Overlapping the DIC strain result and the near-infrared images we could see where the deformation and the failure occurred.

Values of shear strain obtained for every image frame allow us to calculate the shear strain rate and the shear modulus of the weak layer. A fit of shear strain and time provided the shear strain rate. Similarly, we obtained the shear modulus from a regression of the shear stress based on the force signal at the load cell and the shear strain.

3. RESULTS

We start by discussing one experiment in more detail before we present results of different weak layer types.

3.1 Shear strain concentrations

Figure 1 shows the sidewall of sample 2, that we tested on 1 July 2018. The near-infrared picture highlights the weak stratigraphy of a layer of decomposing fragmented particles which is embedded between stiffer layers above and below. This stratigraphy led to a concentration of high shear strain during the stress build up. Overlapping the DIC strain analysis and the near-infrared picture confirmed that the deformation and eventually the failure occurred in the weak layer.

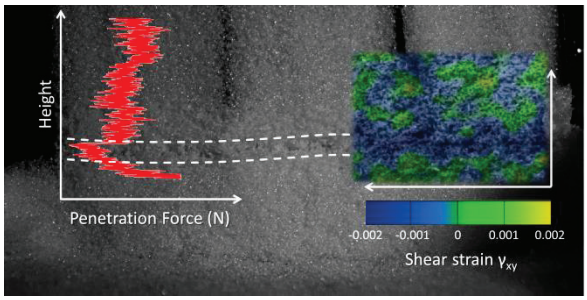

Figure 1: Near-infrared picture of shear experiment overlain with SMP signal (red) and DIC shear strain analysis (color scheme). Two dashed lines embrace the weak layer.

To estimate the concentration of the shear strain in the weak layer we calculated a ratio comparing the shear strains in the slab and the weak layer. In this case the shear strain in the slab reached, at most, 6% of the shear strain ob-

served in the weak layer. In other words, before failure the shear strain in the weak layer was at least 16 times higher than in the slab layer above.

3.2 Failure

Brittle failure is marked by an abrupt drop of stress. In Figure 2 we observe such a sharp transition suggesting the failure is brittle. However, the measurements of stress and displacement shown in Figure 2 refer to the entire sample, i.e. the measurement of displacement summarizes the deformation of the entire sample, including the slab and the weak layer. On the contrary, the DIC technique allows focusing on the weak layer.

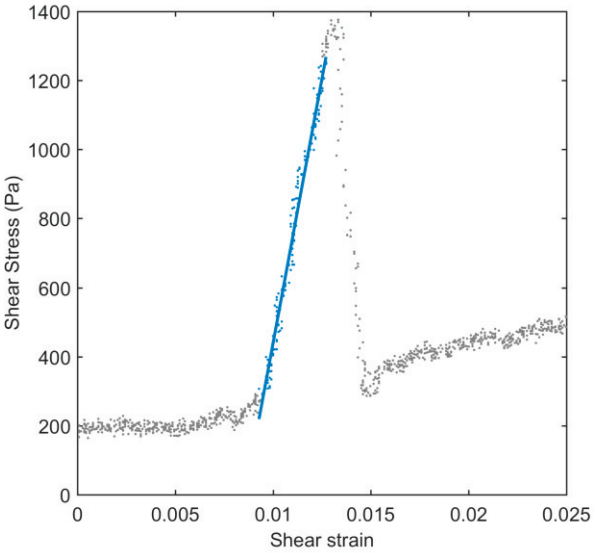

Figure 2: Shear stress and small shear strain measured on the entire sample. The slope of the blue regression illustrates stiffness (0.3 MPa).

Figure 3 shows that, contrary to Figure 2, plastic deformation occurred in the weak layer. Failure occurred at a shear strain of about 0.0015, but the stress did not increase above a shear strain of 0.001.

We describe this failure characteristic with the amount of non-recoverable strain energy per unit volume. In this case, the amount of elastic strain energy per unit volume that is not recoverable (orange area) was 26% of the total strain energy per unit volume (strain energy intensity). Hence, failure was not purely brittle but occurred after some plastic deformation, indicating ductility.

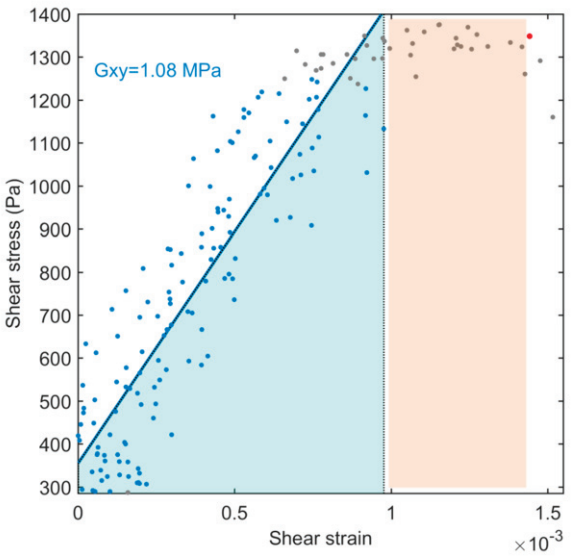

Figure 3: Stress and strain measured in the weak layer with digital image correlation. The slope of the blue regression line illustrates the shear modulus G_{xy}. The blue area represents the theoretical recoverable portion of the strain energy intensity, while the orange portion is non-recoverable.

3.3 Different weak layers

Table 1 compiles the results we obtained for the three different weak layers (DF, SH, and FC(xr)). Shear strength values were on the order of 1 kPa, shear moduli were around 1 MPa and strain rates around 10^{-3} s^{-1}. Decomposing fragmented particles had the lowest average values of shear strength and shear modulus, but generally speaking, variations between different weak layer types were not very pronounced. In all experiments we observed a concentration of the shear strain in the weak layer ultimately leading to failure after plastic deformation and strain softening.

Table 1: Summary of the results for different weak layer types.
Average values for every weak layer type and the standard deviation are provided.

Weak layer type	Shear Strength (kPa)	Shear Modulus (MPa)	Strain rate (10^{-3} s^{-1})	Strain in weak layer (%)	Non-recoverable strain energy intensity (%)
SH	1.4 ± 0.4	1.2 ± 0.6	2.3 ± 1.8	90 ± 6	23 ± 17
DF	1.0 ± 0.2	0.8 ± 0.4	2.8 ± 2.1	93 ± 4	20 ± 12
FC(xr)	1.3 ± 0.3	1.7 ± 1.0	1.1 ± 0.5	86 ± 10	14 ± 10

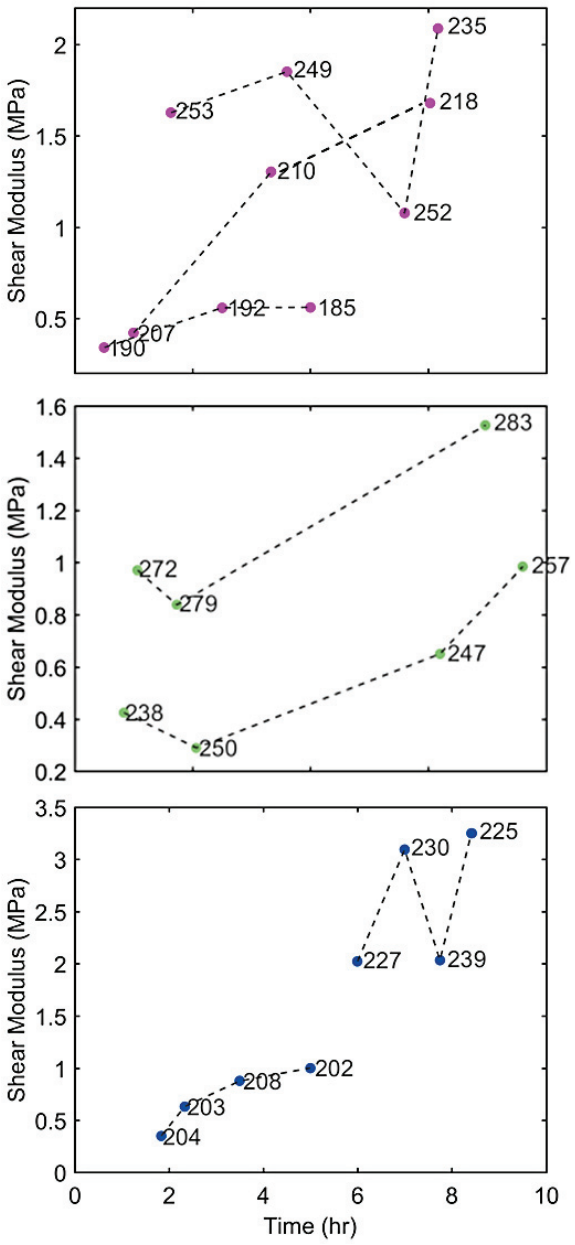

Figure 4: Temporal evolution of shear modulus for surface hoar (top), decomposing fragmented particles (center) and (rounding) facets (bottom). Values associated with each of the data points indicate weak layer density (kg m^{-3}).

3.4 Temporal trends

Whereas variations across weak layer types were rather small, we observed trends between the samples of a certain weak layer type over time. Figure 4 shows time series of weak layers of surface hoar (SH), decomposing fragmented particles (DF), and (rounding) faceted crystals (FC(xr)). In our experiments we observed that the shear modulus increased with time. This increase was strongest for decomposing particles and weakest for rounding facets.

While the shear strength also increased with time in decomposing fragmented particles, surface hoar and (rounding) facets did not show a significant change with time.

The reasons for these trends seem rather independent of weak layer densification as values of weak layer densities remained mostly unchanged. The trends are rather due to sintering.

4. DISCUSSION

To understand changes in mechanical properties and snow microstructure in weak layers after burial we sheared small layered snow samples, similar to the experiments of Walters and Adams (2012). In accordance with their experiments we found the shear strain to concentrate in a band which we identified as the weak layer in near-infrared pictures. We obtained this result across all tested weak layer types.

The samples were sheared at a strain rate of 10^{-3} s^{-1}, which would be in the brittle range according to former studies on samples in shear (Joshi et al., 2006; Schweizer, 1998). Although all of our measurements using the entire sample indicated brittle failure, we determined considerable plastic deformation in the weak layer before failure, indicating ductility. Based on the DIC analysis non-recoverable strain energy per unit volume was around 20% and slightly lower in facets.

With regards to the different weak layer types, we found that just after burial shear modulus and strength of decomposing fragmented particles are similar to the properties of persistent grain types, but they stiffen and strengthen faster.

Overall, shear modulus increased over time for all types of weak layers. A less pronounced increase was also observed for shear strength but only for the decomposing fragmented particles similar to the results of Podolskiy et al. (2014). These trends indicate that decomposing fragmented particles strengthen and stiffen in the hours after burial.

Densification alone cannot explain the increase in modulus and strength we observed. This suggests that parameterizations of mechanical properties based on density only are not always sufficient, confirming earlier results (e.g. Srivastava et al., 2016).

As the samples were exposed to a constant snow temperature of -5°C isothermal metamorphism occurred and the snow microstructure developed towards more rounded structures and larger bonds (sintering) without changing its density (e.g. Kaempfer & Schneebeli, 2007). Such developments of the microstructure likely form stronger and stiffer snow.

5. CONCLUSIONS

We performed shear experiments on small snow samples containing weak layers of surface hoar, decomposing fragmented and faceted crystals at shear strain rates of about 10^{-3}. Across all weak layer types, we observed a pronounced strain concentration in the weak layer and undeniable plastic deformation before failure.

Values of shear strength and shear modulus did not vary much between weak layer types. In fact, in our samples shear strength was around 1 kPa and shear modulus around 1 MPa.

However, within one weak layer type variations of shear strength and shear modulus increased partly related to the lag times between sample preparation and testing. While increasing trends of modulus and strength were not related to densification, sintering is likely the force behind the observed trends as samples were kept at -5°C causing isothermal metamorphism.

ACKNOWLEDGEMENT

B.R. has been founded by the Swiss National Science Foundation (P2EZP2_168896).

REFERENCES

Joshi, S. K., Mahajan, P., & Upadhyay, A. (2006). *Study of layered snow under shear and tension*. Paper presented at the Proceedings ISSW 2006. International Snow Science Workshop, Telluride CO, U.S.A., 1-6 October 2006.

Kaempfer, T. U., & Schneebeli, M. (2007). Observation of isothermal metamorphism of new snow and interpretation as a sintering process. *Journal of Geophysical Research-Atmospheres, 112*(D24), D24101. <Go to ISI>://WOS:000251878400008

Löwe, H., & van Herwijnen, A. (2012). A Poisson shot noise model for micro-penetration of snow. *Cold Regions Science and Technology, 70*, 62-70.

Podolskiy, E. A., Barbero, M., Barpi, F., Chambon, G., Borri-Brunetto, M., Pallara, O., et al. (2014). Healing of snow surface-to-surface contacts by isothermal sintering. *The Cryosphere, 8*(5), 1651-1659. http://www.the-cryosphere.net/8/1651/2014/

Proksch, M., Reuter, B., Löwe, H., Schweizer, J., & Schneebeli, M. (2014). *Quantitative snow stratigraphy and stability derived from high-resolution penetrometry.* Paper presented at the Proceedings ISSW 2014. International Snow Science Workshop, Banff, Alberta, Canada, 29 September - 3 October 2014.

Schweizer, J. (1998). Laboratory experiments on shear failure of snow. *Annals of Glaciology, 26*, 97-102.

Schweizer, J., Reuter, B., van Herwijnen, A., & Gaume, J. (2016). *Avalanche release 101.* Paper presented at the Proceedings ISSW 2016. International Snow Science Workshop, Breckenridge CO, U.S.A., 3-7 October 2016.

Srivastava, P. K., Chandel, C., Mahajan, P., & Pankaj, P. (2016). Prediction of anisotropic elastic properties of snow from its microstructure. *Cold Regions Science and Technology, 125*, 85-100. http://www.sciencedirect.com/science/article/pii/S0165232X16300052

Stanton, B., Miller, D., & Adams, E. (2012). Analysis of Surface Hoar Growth Under Simulated Meteorological Conditions. *Proceedings, 2012 International Snow Science Workshop, Anchorage, Alaska*.

Walters, D. J., & Adams, E. E. (2012). *Directional mechanical properties of radiation recrystallized snow layers from experimental testing.* Paper presented at the Proceedings ISSW 2012. International Snow Science Workshop, Anchorage AK, U.S.A., 16-21 September 2012.